Journal of Nano- and Electronic Physics
Vol. **9** No 4, 04019(6pp) (2017)

Журнал нано- та електронної фізики
Том **9** № 4, 04019(6cc) (2017)

Development of Numerical Method for Optimizing Silicon Solar Cell Efficiency

E. Chahid[1,2], M. Fedaoui[2], M. Nachaoui[3], N.R. Chowdhury[4], A. Malaoui[1]

[1] *Laboratoire Interdisciplinaire de Recherche en Sciences et Techniques (LIRST), Faculté Polydisciplinaire, Université Sultan Moulay Slimane, Beni Mellal, Morocco*
[2] *Laboratory of energy engineering, Materials and systems National School Applied Sciences, University Ibn Zohr, Agadir, Morocco.*
[3] *Laboratory of Applied Mathematica, Sultan Moulay Slimane University, Beni Mellal, Morocco*
[4] *Department of Energy System Engineering, Institute of Energy Studies, University of North Dakota, USA*

(Received 18 April 2017; revised manuscript received 25 July 2017; published online 27 July 2017)

This paper presents a development of numerical method to determine and optimize the photocurrent densities in silicon solar cell. This method is based on finite difference algorithm to resolve the continuity and Poisson equations of minority charge carriers in *p-n* junction regions by using Thoma's algorithm to resolve the tridiagonal matrix. These equations include several physical parameters as the absorption coefficient and the reflection one of the material under the sunlight irradiation of $AM_{1.5}$ solar spectrum. In this work, we study the effect of various parameters such as thickness and doping concentration of the (emitter, base) layers on crystalline silicon solar cell perfomance. The obtained results show that the optimum energy conversion efficiency is 22.16 % with the following electrical parameters solar cell $V_{oc} = 0.62$ V and $J_{ph} = 43.20$ mA·cm^{-2}. These results are compared with experimental data and show a good agreement of our developped method.

Keywords: Photocurrent density, Solar cell, Efficiency, Finite difference method, Tridiagonal matrix.

DOI: 10.21272/jnep.9(4).04019 PACS numbers: 73.40.Lq, 84.60.Jt

1. INTRODUCTION

Crystalline and amorphous silicon solar cells are considered by many researchers to be the most promising energy generation technology, and become the dominant photovoltaics (PV) technology for the future. Because silicon exhibits good stability, a well balanced set of physical and electronic popreties [1-3]. However, cost reduction is the main challenge for Si solar cells due to the use of expensive silicon wafer substrates cut and the requirement of high temperature processing during junction formation [4-8].
Improvement of the efficiency of silicon solar cells is an essential requirement if the technology is to remain competitive with other PV technologies. Nowaday, the solar cells based on silicon have achieved efficiencies of around 20-25 % [9-15].

The principal parameters of solar cell are the following: depth of layers, doping concentration and the layer of Back Surface Field (BSF), minority carrier lifetime, defect recombination, band gap, and resistivity. These parameters are curcial factors that influence the solar cell performance. Furthermore, the photovoltaic cells performance is determined from their current-voltage characteristic under illumination $AM_{1.5}$. Also, it strongly depends on the open circuit voltage, the short-circuit current, and on the Fill Factor (FF) [16-20]. In order to obtain high efficiency, it is necessary to optimize the cell's parameters either experimentally or by simulation. Experimental optimization has, on the one hand, the advantage of being real, and on the other hand, it is tiresome, costly, and it does not give us access to certain cell parameters. Concerning simulation optimization, as it follows a mathematical model more or less close to the real system, we can say that it is getting easy, cheaper, inexpensive and allows access to any parameter of the cell [21-23].

The analytical expression for photocurrent can be found assuming simplified conditions in the different regions. But, we can notice some difficulties on the level of the determination of the electrical parameters' solutions especially in the deplition region. Indeed, the electric field is not negligible and often the resolution of these equations is done in an approximate solution. It also can not directly determine the following physical quantities as the built-in potential, band energy and charge carrier density. In parallel, a numerical method can be done to solve an exact continuity and Poisson's equations in the different cell regions. The used Finite Difference Method (FDM) is developed to find accurate results of carriers minority densities in a p-n junction [24, 25]. This method follows Thomas's algorithm which is specific to the resolution of the tridiagonal matrix. The proposed numerical method is tested and analyzed by comparing the found results with experimental data [26, 27].

This work deals with the cell parameters optimization by following a numerical model of the physical and geometrical parameters of the different layers of a Silicon photovoltaic solar cell (Si). The high efficiency device is determined by accurate analysis of the impact of the thichkness and doping concentrations impurity of the emitter and base layers cell.

2. MODELING OF P-N SOLAR CELL

The *p-n* solar junction is formed of two region types p and n deposed on the metallic substrate aluminum (Al) as the back and front contacts. A diagram of this structure is illustrated in Fig. 1, the table 1 regroups the physical parameters used in simulation. This structure was studied under solar spectrum $AM_{1.5}$, with incident light power per unit area of a surface is equal to $P = 100$ mW/cm^2 and at room temperature $T = 300$ K.

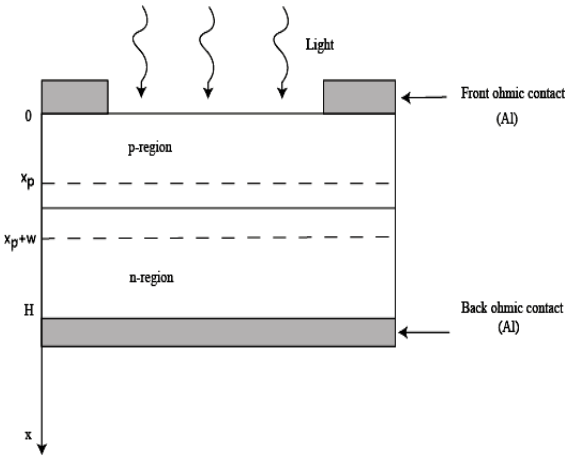

Fig. 1 – Schematic illustration of a *p-n* solar cell structure

The total photocurrent J_{ph} results from the sum of the three components, the drift current of the electrons J_n in the p type region, the drift current of the photoholes J_p in the n type region and the photogeneration J_g in the space charge region (SCR). This latter is constituted by J_{gn} and J_{gp} in the space region beside P region and N region respectively: $J_g = J_{gn} + J_{gp}$
For a wavelength (λ), the cell photocurrent is :

$$J_{ph}(\lambda) = J_n(\lambda) + J_g(\lambda) + J_p(\lambda) \tag{2.1}$$

The total photocurrent trough the cell is the result of integration of all solar spectrum:

$$J_{ph}(\lambda) = \int_{\lambda_{\min}}^{\lambda_{\max}} J_{ph}(\lambda)\, d\lambda \tag{2.2}$$

The characteristic J(V) of the cell with is written as follows:

$$J = J_{ph} - J_s\left(\exp(\frac{qv}{k_B T}) - 1\right) \tag{2.3}$$

Where, q is the charge of the electron, T is the cell temperature, k_B is the Boltzmann's constant and J_s is the saturation current written as in the case of the p^+-n junction :

$$J_s = \frac{qn_i^2 D_p}{N_d L_p}\ (A/cm^2) \tag{2.4}$$

Where n_j, D_p, N_d, L_p and D_p are respectively the intrinsic density, donor concentration, and both the diffusion length and diffusion coefficient of holes.

3. THEORY

The basic equations for semiconductors device can be classified in three groups; for one- dimensional case [26]:

$$\text{Poisson's equation: } \frac{\partial E}{\partial x} = \frac{\rho}{\varepsilon} \tag{3.1}$$

- Current densities equations:

$$J_n = q\mu_n nE + qD_n \frac{\partial n}{\partial x} \tag{3.2}$$

$$J_p = q\mu_p pE - qD_p \frac{\partial p}{\partial x} \tag{3.3}$$

- Continuity equations:

$$\frac{\partial n}{\partial t} = G_n - R_n + \frac{1}{q}\frac{\partial J_n}{\partial x} \tag{3.4}$$

$$\frac{\partial p}{\partial t} = G_p - R_p - \frac{1}{q}\frac{\partial J_p}{\partial x} \tag{3.5}$$

The generation rate $G(x, \lambda)$ at position (x) is determined by the Beer-Lambert law relating to incident flux $F(\lambda)$, reflectivity $R(\lambda)$, and absorption coefficient $\alpha(\lambda)$ as:

$$G(x, \lambda) = \alpha(\lambda)(1 - R(\lambda))F(\lambda)\exp(-\alpha(\lambda)x) \tag{3.6}$$

The recombination rate $R(x, \lambda)$ at position (x) in the p -type semiconductor is described by:

$$R(x, \lambda) = \Delta n(x, \lambda)/\tau_n \tag{3. 7}$$

Where Δn is the minority excess concentration of electrons in the p-type semiconductor with respect to the equilibrium concentration n_{p_0} and τ_n is the minority electrons lifetime, $\Delta n\ (x, \lambda) = n_p\ (x, \lambda) - n_{p0}\ (x, \lambda)$. The hole recombination rate R_p in the quasi-neutral region of the n-type semiconductor is given by the same equation cited aboven only we subtitute n by p.

In order to determine the total photocurrent we solve the continuity equations of electrons and holes in each region of the cell.

In the case of the permanent mode, the continuity equation of electrons in the emitter region of the cell is written by (case of holes continuity equation in the base region can treated similarly):

$$D_n \frac{d^2 n}{dx^2} - \frac{\Delta n}{\tau_n} = -\alpha(\lambda)(1 - R(\lambda))F(\lambda)\exp(-\alpha(\lambda)x) \tag{3.8}$$

The boundary conditions, in the emitter region, at the two edges satisfy the following equation [28]:

- At the top contact ($x = 0$):

$$S_n \Delta n = D_n \left.\frac{\partial n}{\partial x}\right|_{x=0} \tag{3.9}$$

Where S_n is the surface recombination velocity.

- At the junction edge side ($x = x_p$):

$$\text{n}{=}n_{p_0} = \left.\frac{n_i^2}{N_a}\right|_{x=x_p} \tag{3.10}$$

The photocurent density due to the diffusion charge carrier is obtained by the following formula:

$$J_n = qD_n \left.\frac{\partial n}{\partial x}\right|_{x=0}, \text{ and } J_p = -qD_p \left.\frac{\partial p}{\partial x}\right|_{x=x_p} \tag{3.11}$$

In the SCR region, the electric field in the *p*-*n* Junction, is obtained by solving the Poisson's equation:

$$E(x)=\begin{cases}-\dfrac{qN_a}{\varepsilon}(x-x_p); x_p<x<x_p+x_r\\ \dfrac{qN_d}{\varepsilon}(x-(x_p+W)); x_p+x_r<x<x_p+W\\ 0; \qquad\qquad otherwise.\end{cases} \quad (3.12)$$

The expression of the space charge width area W is such that:

$$W=\sqrt{\frac{2\varepsilon_0\varepsilon_r}{q}(\frac{1}{N_a}+\frac{1}{N_d})V_d} \quad (3.13)$$

At the potential difference between the bands, an internal potential difference referred to as the diffusion potential barrier V_d is expressed as:

$$V_d=V_t\ln\left(\frac{N_aN_d}{n_i^2}\right) \quad (3.14)$$

Where, V_t is the thermal voltage which equal 26 mV. Both the D_n, D_p with ($cm^2\cdot s^{-1}$), can be written as [21]:

$$D_n=1350V_t/(1+81N_a/(N_a+3.2\times10^{18}))^{1/2} \quad (3.15)$$

$$D_p=480V_t/(1+350N_d/(N_d+1.05\times10^{19}))^{1/2} \quad (3.16)$$

The minority carrier lifetimes τ_n, τ_p with unity (μs), are empirically expressed as [21]:

$$\tau_n=12/(1+N_a/5\times10^{16}) \quad (3.17)$$

$$\tau_p=12/(1+N_d/5\times10^{16}) \quad (3.18)$$

At equilibrium state, equations (9) and (10) reduced to the following differential equations for electrons and holes:

$$D_n\frac{d^2n}{dx^2}+\mu_nE\frac{dn}{dx}+n\mu_n\frac{dE}{dx}+G_n-\frac{\Delta n}{\tau_n}=0 \quad (3.19)$$

$$D_p\frac{d^2p}{dx^2}-\mu_pE\frac{dp}{dx}-p\mu_p\frac{dE}{dx}+G_p-\frac{\Delta p}{\tau_p}=0 \quad (3.20)$$

The boundary conditions in the depletion region are:

$$\Delta n(x=x_p)=0;\ n(x_p)=n_{p_0} \quad (3.21)$$

$$\Delta n(x=x_p+W)=0;\ n(x=x_p+W)\approx N_d \quad (3.22)$$

An analogous expression the holes can be found by replacing n by p and n_0 by p_0 in *E*q. (3.21, 3.22).

4. DEVELOPMENT OF NUMERICAL METHOD

The finite difference method is a numerical method to solve linear differential equations using finite difference approximations of the derived functions $u(x)$.

The interval [0, H] is divided into ($M+1$) sub interval with steps $h=H/(M+1)$. Thus, we search the solution at grid points in space $(x_i)_{1\le i\le M}$. We will use the notation (u_i) to denote the value of the function $u(x_i)$ at the i-th node of the computational grid.

In general, the Taylor's formula, at the first and second order, can be used to approximate the derivate of a function $u(x)$ with centered differences around the points ($i\pm1$) of the interleaved mesh:

$$\begin{aligned}&du/dx(x_i)\approx(u_{i+1}-u_{i-1})/2h\\ &(d^2u)/(dx^2)(x_i)\approx((u_{(i+1)}-2u_i+u_{(i-1)}))/h^2\end{aligned} \quad (4.1)$$

The continuity equations of the minority carriers can be discretised in the following form (case of holes can be treated similarly):

$$a_iu_{i-1}+b_iu_i+c_iu_{i+1}=d_i \quad (4.2)$$

This equation can be written in a tridiagonal matrix form and is solved using the Thomas's algorithm [26]. The coefficients a_i, b_i, c_i and d_i are given in the different regions of the solar cell as follows:

- **In the neutral charges *N* and *P* ($0<x<x_p$):**

In the *n*-type region, the obtained coefficients are:

$$a_i=1,\ b_i=-(2+h^2/L_n^2),\ c_i=1, \text{ and } d_i=h^2G(x_i)/D_n \quad (4.3)$$

The same coefficients in the *p*-type region ($x_p+W<x<H$), only we subtitute L_n, D_n with L_p, D_p respectively.

- **In the space charge region ($x_p<x<x_p+W$):**

We can distinguish between two regions:

- The first is juxtaposed with *p*-type region ($x_p<x<x_p+x_r$):

The obtained coefficents are:

$$\begin{cases}a_i=(1-\mu_nhE(x_i)/2D_n),\ b_i=\\ =-(2+h^2(q\mu_nN_a/\varepsilon D_n+1/L_n^2))\\ c_i=(1+\mu_nhE(x_i)/2D_n),\ d_i=\\ =-h^2\left(G(x_i)/D_n+n_{p_0}/L_n^2\right)\end{cases} \quad (4.4)$$

In this region, a density current is generated noted as: J_{scr}^1.

- The second is juxtaposed to *n*-type region ($x_p+x_r<x<x_p+W$):

We obtained the same coefficients related to the holes, but only we subtitute N_a, μ_n, L_n and D_n with $-N_d$, μ_p, L_p and D_p. Here, the holes produce a density current noted as: J_{scr}^2.

For a wavelength (λ), the light-generated current J_{scr} is:

$$J_{scr}=J_{scr}^1+J_{scr}^2 \quad (4.4)$$

The obtained equations are a linear system can be written in matrix form as follows:

$$Au=B \quad (4.5)$$

The (u) values can be obtained by using Gauss Seidel's method [29].

5. RESULTS AND DISCUSSIONS

In this study, the obtained results and literature values of the physical parameters are illustrated in the Table 2. In order to validate our developed method, we have presented, on the one hand, the experimenal data of studied material [30, 31]. These data are analyzed and introduced in the developed equations to extract interesting informations on properties in this field. On parameters by our method are presented and compared to the theory [21].

5.1 Experimental Data

In this work, the absorption coefficient for silicon semiconductor material is shown in the figure below. Accurate modeling of Silicon solar cell requires more detailed knowledge of the absorption coefficient [30, 31].

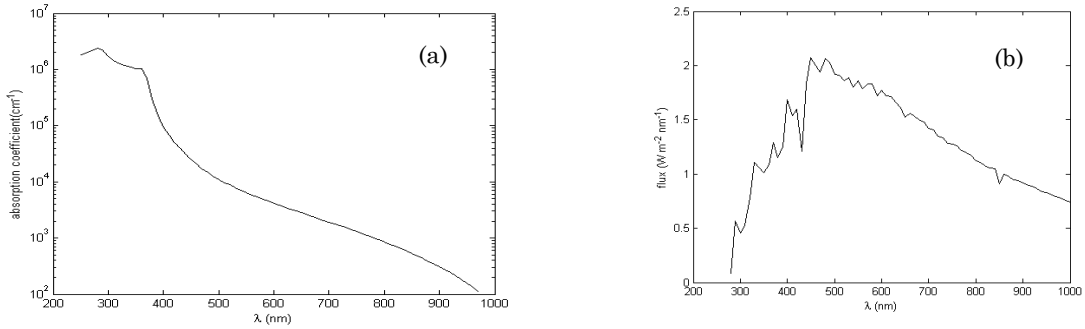

Fig. 2 – Variation of both silicon absorption coefficient (a), and flux of sunlight (b) versus wavelength

Table 2 – Parameters set for numerical calculation of *p-n* Si junction [21]

Parameters	Value
Emitter thickness (μm)	2
Base thickness (μm)	250
Acceptor doping (cm^{-3})	$5 \cdot 10^{17}$
Donor doping (cm^{-3})	$5 \cdot 10^{16}$
Diffusion potential barrier (V)	0.83
Electron diffusion coefficient D_n ($cm^2 \cdot s^{-1}$)	10.1
Hole diffusion coefficient D_p ($cm^2 \cdot s^{-1}$)	7.61
Electron mobility μ_n ($cm^2 \cdot V^{-1} \cdot s^{-1}$)	$1.5 \cdot 10^3$
Hole mobility μ_p ($cm^2 \cdot V^{-1} \cdot s^{-1}$)	$4.5 \cdot 10^2$
Electron lifetime τ_n (μs)	1.09
Hole lifetime τ_p (μs)	6
Electron recomb. velocity S_n ($cm \cdot s^{-1}$)	10^2
Hole recomb. velocity S_p ($cm \cdot s^{-1}$)	10^6

5.2 Results of Electrical Parameters

The developed method based on FDM allows the determination of the densities currents in each region of the studied semiconductor. Using the equations (3.1-3.5), the currents densities (J_{ph}, J_{scr}, J_p and J_n) are calculated and represented as a function of the wavelength (λ) in Fig. 3. Many interesting information are extracted from this figure, which are regrouped in three points; firstly, we note that there is two critical values of (λ) which are: $\lambda_{max} \approx 0.69\mu m$ corresponds to a maximum of J_{ph} and $\lambda_{tresh} \approx 0.56\mu m$ represents the maximum limit of J_n linearity. Secondly, the *n*-type region participates for the production of the current with a percentage of 40 % when $\lambda > \lambda_{max}$ and often this layer is less considered during the improvement of the photovoltaic cell performance. While $\lambda < \lambda_{tresh}$, only *p*-type region contribute to generate the current with a linear manner. Finally, the total photocurrent J_{ph} is relatively low, when we get the other hand, the found electrical

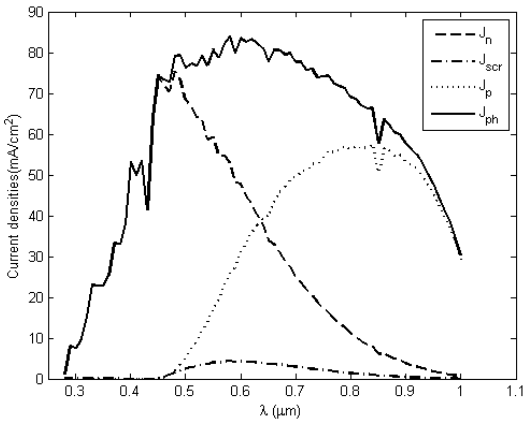

Fig. 3 – Current densities as a function of wavelength

near to UV spectrum. Therefore, the reason laying behind using technological techniques in the cells' industry is to add both a window layer on silicon single *p-n* junction and another one such as SiO_2 in order to passivate the produced silicon cell.

In table 3, we present the components of densities currents calculated by FDM and also the value of open circuit necessary to calculate the conversion efficient η which equal 23.09 %. As shown, the most dominant current density relative to *p*- region is J_n; whereas, the contribution of deplition layer is small.

Table 3 – Values of determined current densities

Current densities ($mA \cdot cm^{-2}$)	J_p	J_g	J_n
FDM values	21.07	1.18	18.47

In Table 4, the total photocurrent J_{ph} is calculated using FDM and compared to both the analytical model [21] and the experimental data [13]. We observe that the results values are closer to the experimental ones and the difference between them is about 2.5 %. The obtained results are significantly better relatively to the analytical model refering to the experimental data.

Table 4 – Comparison of photovoltaic parameters in *p-n* Si solar cell

	Developed Method	Theortical Model	Experimental data
J_{ph} (mA·cm^{-2})	40.72	35.4	39.8
V_{oc} (V)	0.63	0.62	0.66
η (%)	21.46	17.5	21.3

Indeed, a simplification is used in the analytical model during the resolution of differential equation. In order to have a good performance of solar cell structure, an optimization is necessary on the level of the emitter and the base layers' thickness X_p, X_n and doping N_a, N_d respectively.

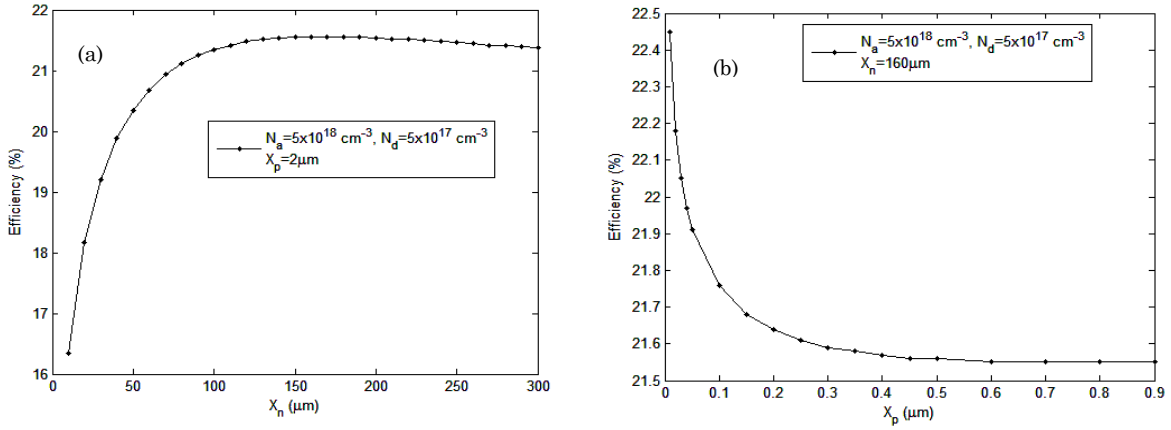

Fig. 4 – Variation of the efficiency as a function of base thickness X_n (a), and emitter thickness X_p (b)

Figure 4 shows the results of the energy conversion efficiency variation as a function of *p*-region thickness X_n and *p*-region thickness X_p. As we can see in Fig. 4a, the efficiency is increased with the increase of the base thickness and the optimal thickness is $X_n = 160$ μm which leads to obtain a Maximum Efficiency Point (MEP) value of 22.45 %. While, the efficiency is decreased rapidly when the thickness of the emitter is increased as shown in Fig. 4b and an optimal thickness is $X_p = 0.01$ μm which corresponds to MEP of $\eta = 21.56$ %.

The variation of the conversion efficiency versus both the doping acceptors and donors is presented in Figure 5. We notice in Fig. 5a, that when the acceptor concentration increases, the efficiency decreases rapidly. In Fig. 5b, we notice that the efficiency slightly decreases whenever the donor concentration increases. We have obtained the $N_a = 10^{18}$ cm^{-3} and $N_d = 4 \cdot 10^{16}$ cm^{-3} as the optimal doping concentration. They lead to achieve a maximum energy conversion efficiency equal to 22.16 %. The electrical parameters values correspanding to the above obtained efficiency are $V_{oc} = 0.62$ V and $J_{ph} = 43.20$ mA·cm^{-2}. This result will be realized by using the nanotechnologies products or to be more specific nanomaterials with higher absorption coefficient of the light spectrum.

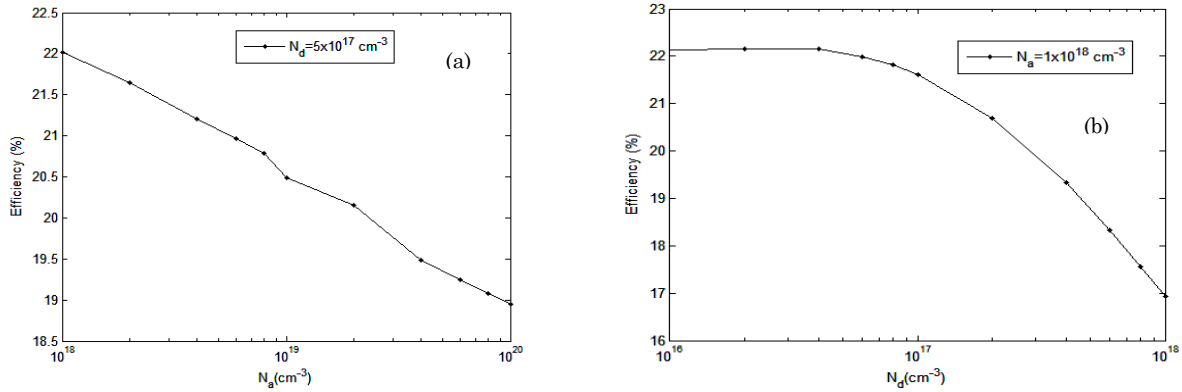

Fig. 5 – Variation of the efficiency as a function of the emitter (a), and base doping regions (b)

6. CONCLUSION

In this work, a numerical method is developed to determine physical and electrical quantities of crystalline silicon solar cells using the finite difference method. The discretization of minority carriers continuity and Poisson's equations allow to determine the current density components in different regions. After analyzing these currents, we conclude that the region responsible for producing the most photoelectric is the emitter layer. The obtained results are compared with the experimental data, and reveals that the achieved cell conversion efficiency is 21.46 %. This latter value is better than those obtained by analytical model about

4.46 %, showing that the our developed method is efficient. Consequently, the found optimal physical and geometrical parameters of the studied cell are $X_p = 0.01$ μm, $X_n = 160$ μm, $N_a = 10^{18}$ cm^{-3} and $N_d = 4 \cdot 10^{16}$ cm^{-3}. These values lead to achieve a cell efficiency of 22.16 % with the following electrical parameters $V_{oc} = 0.62$ V and $J_{ph} = 43.20$ mA·cm^{-2}, and show an improvement in the silicon photovoltaic cell efficency.

REFERENCES

1. W.G. van Sark, L. Korte, F. Roca, *Physics and technology of amorphous- crystalline heterostructure silicon solar cells* (Berlin Heidelberg: Springer-Verlag: 2012).
2. E. Chahid, M. Oumhanad, M. Feddaoui, A. Malaoui, *J. Ovonic. Res.* **13** No°3, 119 (2017).
3. G. Watt, H. Fechner, *Elektrotech. Inf. Tech.* **126** No 9, 328 (2009).
4. W.G. van Sark, P. Muizebelt, J. Cace, A. de Vries, P. de Rijk, *Renew. Energy* **71**, 18 (2014).
5. E. Chahid, O. Idali, M. Fedaoui, M. Eritali, A. Malaoui, *Int. J. Elec. Comput. Eng.* **7** No 1, 50 (2017).
6. N. Memarian, M. Minbashi, M. Jalali Mehrabad, *J. Nano-Electron. Phys.* **8**, No 4(2), 04058 (2016).
7. M. Bazilian, I. Onyeji, M. Liebreich, I. MacGill, J. Chase, J. Shah, D. Gielen, D. Arent, D. Landfear, S. Zhengrong, *Renew. Energy* **53**, 329 (2013).
8. C. Budischak, D. Sewell, H. Thomson, L. Mach, D.E. Veron, W. Kempton, *J. Power Sources* **225**, 60 (2013).
9. N. Hernandez-Como, A. Morales-Acevedo, *Sol. Energ. Mater. Sol. C.* **94** No 1, 62 (2010).
10. J. Zhao, *Sol. Energ. Mater. Sol. C.* **82** No 1-2, 53 (2004).
11. M. Tanaka, S. Okamoto, S. Tsuge, S. Kiyama, *3-rd World Conference on Photovoltaic Energy Conversion (WCPEC-3)*, 955, (Japan: Kosuke Kurokawa: 2003).
12. S. Taira, Y. Yoshminine, T. Baba, M. Taguchi, H. Kanno, T. Kinoshita, H. Sakata, E. Maruyama, M. Tanaka, *22nd European Photovoltaic Solar Energy Conference,* 932, (Italy: 2007).
13. M.A. Green, K. Emery, Y. Hishikawa, W. Warta, E.D. Dunlop, *Prog. Photovolt. Res. Appl.* **23**, 1 (2015).
14. M. Hofmanm, S. Janz, C. Schmidt, S. Kambor, D. Suwito, N. Kohn, J. Rentsch, R. Preu, S.W. Glunz, *Sol. Energ. Mater. Sol. C.* **93**, 1074 (2009).
15. L. Jia, H. Shihua, H. Lü, *J. Semicond.* **36** No 4 (2015).
16. N. Dwivedi, S. Kumar, A. Bisht, *Sol. Energy.* **88**, 31 (2013).
17. B. Dennai, H. Ben Slimane, A. Helmaoui, *J. Nano- Electron. Phys.* **6** No 4, 04001 (2014).
18. Q. Liu, X.J. Ye, C. Liu, *Optoelectron. Lett*, **6**, 108 (2010).
19. A. Malaoui, E. Barrah, J. Antari, *Int. J. Innov. Appl. Stud.* **15**, 329 (2016).
20. J.J. Liou, W.W. Wong, *Sol. Energ. Mat. Sol. C.* **28**, 9 (1992).
21. A. Malaoui, *Int. J. Innov. Appl. Stud.* **18** No 1, 328 (2014).
22. H. Eschrich, J. Bruns, M.E. Nell, B. Reinicke, H.G. Wagemann, *10 th European Photovltaic Solar Energy Conference,* (Lisbon Portugal: 1991).
23. S.V. Patankar, *Numerical Heat Transfer and Fluid Flow* (New York: Hemisphere/Mc Graw Hill: 1980).
24. M. Kurata, *Numerical Analysis for Semiconductor Devices* (Massachusetts: Lexington Books: 1982).
25. WH. Press, WT. Vettering, S.A. Teukolsky, *Numerical Recipes in C: the Art of Scientific Computing* (Cambridge University Press: 2002).
26. S. Zhang, X. Pan, H. Jia, W. Deng, J. Xu , Y. Chen, P.P. Altermatt, Z. Feng, P.J. Verlinden, *IEEE J. Photovoltaics* **6**, 145 (2016).
27. S.M. Sze, *Phys. Semicond. Dev.* (John Wiley & Sons: 1981).
28. G. Strang, *Linear Algebra and Its Applications* (New York: Academic Press: 1980).
29. S.R. Kurtz, J.M. Olson, A. Kibbler, *Appl. Phys. Lett.* **57**, 1922 (1990).
30. S.R. Kurtz, D.J. Arent, K.A. Bertness, J.M. Olson, *Proceedings of the Compound Semiconductor Epitaxy*, 117 (1994).